Biosensors and Bioelectronics 161 (2020) 112209

Contents lists available at ScienceDirect

Biosensors and Bioelectronics

journal homepage: http://www.elsevier.com/locate/bios

Electrically guided interventional radiology, *in-vivo* electrochemical tracing of suspicious lesions to breast cancer prior to core needle biopsy

Zohreh Sadat Miripour [a,b,1], Parisa Aghaee [a,b], Fereshteh Abbasvandi [c], Parisa Hoseinpour [d], Hadi Ghafari [a], Nasser Namdar [a], Mohammad Esmaeil Akbari [e], Mohammad Abdolahad [a,b,*,1]

[a] Nano Bio Electronic Devices Lab, School of Electrical and Computer Engineering, College of Engineering, University of Tehran, P.O. Box 14395/515, Tehran, Iran
[b] Cancer Electronics Research Group, School of Electrical and Computer Engineering, College of Engineering, University of Tehran, P.O. Box 14395/515, Tehran, Iran
[c] ATMP Department, Breast Cancer Research Center, Motamed Cancer Institute, ACECR, P. O. Box 15179/64311, Tehran, Iran
[d] SEPAS Pathology Laboratory, P.O. Box: 1991945391, Tehran, Iran
[e] Cancer Research Center, Shahid Beheshti University of Medical Sciences, Tehran, Iran

ARTICLE INFO

Keywords:
Electrochemical sensor
Hypoxia
Cancer
Carbon nanotube
Biopsy

ABSTRACT

An electrochemical biopsy probe was designed and fabricated to detect cancer tumors under the sonography guide without the need for any sample dissection (biopsy). The system was based on recording the hypoxic function of cancer tumors by Multi-wall carbon nanotubes (MWCNTs) sensing agents had been decorated on the tip of the needle electrodes by an electrostatic deposition method. This system named BGP successfully distinct 4T1 and MC4L2 breast tumors from normal lesions. It also diagnosed the treated tumors from vital ones. BGP as a clinically useful biosensor would detect the cancerous probability of any suspicious breast mass without any sample excision. Also, it can present a profile from neoplastic states of different regions of a tumor. This ability would make ensure for the radiologist to do biopsy or not, especially in the cases which are suspicious between BIRADS III and IVa. This would not only shed new light in detecting breast cancer tumors without biopsy (applied in radiological BIRADS classifications) but also evaluate the therapeutic effects on cancer tumors after chemotherapy/radiotherapy therapies without complicated and expensive scanning.

1. Introduction

Women are mostly diagnosed with breast cancer than any other cancers (American Cancer Society. Breast Cancer Facts & Figures 2019–2020). Apart from neoadjuvant therapies, the treatment of cancer typically involves lumpectomy or mastectomy surgeries (Dixon and Barber, 2018). To be ensured from the presence of breast neoplastic tumors in a patient, core needle biopsy would be mandatory to carry out after imaging techniques (such as Mammography, CT-Scan, and sonography) on suspicious solid masses with BIRADS IVa and further (Łukasiewicz et al., 2017). The biopsied samples would be investigated by histopathological and immunohistochemical procedures to achieve final diagnosis on the cancerous probability and grades of the tumors (Ahn et al., 2017), (You et al., 2017). There are several types of biopsies: 1) Fine Needle Aspiration (FNA) biopsy, 2) core (large needle) biopsy, and 3) surgical biopsy. Each of these techniques would be useful depending on the characteristics of the suspected cancerous mass (lesion's level of suspicion, the mass/lump size and location, the presence of other symptoms of lesions) (Ohashi et al., 2016).

Core-needle biopsy, a medical procedure to remove small amounts of suspicious tissue from a lesion or mass with a needle-like cutting system under sonography guide, was introduced in the 1990s, and rapidly replaced fine-needle biopsy (FNA) (Łukasiewicz et al., 2017), (Singh et al., 2016), (Wang et al., 2017). Its growing popularity is due to sufficient sample preparation for accurate diagnosis of benign lesions near distinguishing between *in situ* lesions and invasive carcinoma (Donaldson et al., 2018) with low invasion and seeding probabilities.

Hence, multiple sampling (up to 6) must be done to be ensured from the precision of sampling from misdiagnosis. This would lead to the unavoidable increase of patients' pain and more interventions and stimulation on a crucial location named as tumor active margins (Kılıç et al., 2016).

* Corresponding author. Nano Bio Electronic Devices Lab, School of Electrical and Computer Engineering, College of Engineering, University of Tehran, P.O. Box 14395/515, Tehran, Iran.
E-mail address: m.abdolahad@ut.ac.ir (M. Abdolahad).
[1] Authors with same contributions.

https://doi.org/10.1016/j.bios.2020.112209
Received 3 February 2020; Received in revised form 5 April 2020; Accepted 9 April 2020
Available online 16 April 2020

On the other hand, due to cancer heterogeneity nature, specimens might contain fat necrosis, desmoplasia, or inflammatory cells between cancer cells and cause non-sufficient sampling. Although many in-vivo biosensing methods for cancer detection such as protein-based in-vivo biosensing (Mahr and Frunzke, 2016), (Ehrenworth et al., 2017), Förster resonance energy transfer (FRET)-based biosensor (Peroza et al., 2015), Two-component system (TCS) biosensor (Ravikumar et al., 2017), RNA based biosensors (Rogers et al., 2016), (Zhang et al., 2015), etc. were developed, none of them could be applied in tumor phenotyping. To overcome these problems, scientists have developed different in-vivo tumor bio sensing methods which resulted in many interesting technologies such as Real-Time Bioimpedance-Based Biopsy Needles (Halonen et al., 2019), (Mishra et al., 2012) based on measuring the impedance of suspicious tissue to distinguish normal from suspicious masses. Although it would be so helpful, detecting fibro adenosis lesions contain a rare distribution of malignant cells is a challenge in tissue-based impedance analysis (Zheng et al., 2008). Also, Recently microwave-based in vivo breast imaging was developed to detect cancer tumors in the breast by >1 GHz spectroscopy (Wang, 2018). Dielectric responses of breast tumor and normal regions showed to be different in such frequencies. Moreover, the other technics such as tissue characterization with diffuse reflectance spectroscopy (Spliethoff et al., 2016), Electromagnetic (EM) breast imaging in-vivo (Halter et al., 2009) were reported. Some of the reported advantages and limitations of these techniques were presented in Table S1.

Here we demonstrate an alternative approach for a real-time in vivo detection of the breast tumors suspicious to be atypia, pre-neoplasia or neoplasia by electrochemical tracking the H_2O_2 released during hypoxia assisted glycolysis of suspicious cancerous cells based on an electrochemical recording by carbon nanotube electrodes [US patent pub no Pub. No.: US 2018/0299401 A1, Pub. Date: Oct. 18, 2018] with some modifications which made it suitable for biopsy guidance (named as biopsy guided probe (BGP)).

BGP is the first electrical interventional integrated needles were developed to distinguish BIRADS III from IVa to prevent a non-desired biopsy or to recommend biopsy in crucial cases. As the system has been based on live function of cancer cells (hypoxia glycolysis) its accuracy would be so high. also, a pathological classification was presented for the responses of the sensor based on the animal in-vivo model.

In BGP we changed the mechanical designation of the system to be modified for testing tumors under the sonography. Multiwall carbon nanotube (MWCNT) powder was positively charged by Van de Graaff and electrostatically adhered to Ag paste rubbed on steel needles had been charged by negative electrostatic charges. This made the probe development method remarkably simple and cheap.

BGP was tested on In-vivo animal models with 4T1 and MC4L2 tumors. Also, the effect of tumor treatment by EChT (Electrochemical therapy) methods was rechecked by BGP. The electrochemical results were compared with H&E of biopsied samples, and a comparative table for checking any correlation between BGP responses and pathological diagnostics were presented. Apart from guiding the interventional radiologist to remove the minimal number of samples under CNB, in the future, BGP may be used as an alternative for biopsy.

2. Materials and methods

2.1. Fabrication of BGP for in-vivo assays

First, the sterile needle was rinsed in deionized (DI) water and dried by air. Afterwards, it was covered on the 2 mm from top of the needles by Ag paste, and the rest of them were electrically isolated. Then Van de Graaff electrostatic generator was used to positively charging the CNT and negatively charging the needle. By moving the needle near the CNT powder, the nanotubes were rubbed by the needle and adhered to the top of needles in Ag paste regions (Fig. 1A). After about 10 min, the Ag paste dried, and a CNT decorated needle with good integration, as well as great physical and electrical connections were achieved. CNT's were characterized by Field Emission Scanning Electron Microscopy (FESEM). Fig. 1B shows the FESEM image of the CNT on the needles. Also, other characterizations such as X-ray photoelectron spectroscopy (XPS), Raman, X-ray diffraction (XRD) and Transmission Electron Microscopy (TEM) images of the electrodes decorated by CNT powders, are demonstrated in Fig. S1.

The BGP sensor has the conformation of four electrodes, named Working (WE), Counter (CE), and two Reference (RE) with a distance of 3 mm from each other. Steel needles with a thickness of 0.5 mm used as RE and 250 μm steel needles, which can easily move inside the REs were WE and CE (Fig. 2). We just deposited MWCNTs on the tip of counter and work steel needles. Then needles were attached to an electrical connector with two pins by conductive paste. Computer-aided design (CAD) software was used to design the body of the BGP probe and the 3D printer was applied to build a three-dimensional probe body with ABS (Standard No: ISO 10993) biocompatible material. The connector was fixed inside the body to form the final probe. Then the probe was connected to the readout system by a noiseless cable that handled all electrodes as could be observed in Movie S1. Also, repeatability tests on some randomly selected fabricated sensors with reference solution standard (unstable H_2O_2 contained solution, with the base of lactate (Sigma, CAS. No 79-33-4)) and mice model, were shown in Fig. 1C and Fig. S2A, respectively (horizontal axis: number of the fabricated probe). Well acceptable similarity was observed in responses of the sensors (Fig. 1C).

Supplementary data related to this article can be found at https://doi.org/10.1016/j.bios.2020.112209.

2.2. The electrochemical readout system

The schematic of an integrated portable automatic electrochemical readout board is represented in Fig. 2D. In this system, a low noise, high accuracy, and low power potentiostat equipped by low noise amplifier (LNA) was designed to decrease the loading effect of the environmental noise (Frequency: 0.1Hz to 100 MHz) might be induced by other electrical medical instruments. Moreover, to precisely detect the current signal, flows from the WE to CE, we required a high-speed potentiostat. Hence Current Buffer Amplifier Classes (CBAs) was added to electrical system. The combination of LNA and CBA produces a creative, effective, and appropriate device for high accuracy tests.

On the other hand, Analog to digital (ADC) and Digital to Analog (DAC) converters with 16 bits was applied to increase the accuracy of the readout circuit. A unit of a processor is installed on the board which receives the data of the converters and transmits them via a Bluetooth module to the (Fig. 2D).

Finally, a software was designed based on experimental calibration to analyze the data and diagnose whether the responses are related to cancerous or normal tissues. Not to be neglected that a 3.3V and 800 mA lithium-Ion cell battery is powering all parts of this circuit so it doesn't need to be connected to the external power. This ability of the device provides a free and flexible method for interventional radiologist or surgeon to utilize the device in clinics. For electrochemical measurements, the potential was swept in the range from -0.8 to +0.8 V, using a scan rate of 100 mV s^{-1} as conventional parameters in biological solutions (Shashaani et al., 2016) (Fig. 2E).

2.3. Cell cultures

Mice breast cancer cell lines (MC4L2, 4T1) were obtained from the standard cell banks of the National cell bank (NCBI) located in the Pasteur institute and they were maintained at 37 °C (5% CO_2, 95% air) in RPMI medium (Gibco) supplemented with 5% fetal bovine serum (Gibco), and 1% penicillin/streptomycin (Gibco). The fresh medium was replaced every other day. All cell lines were tested and found negative for Mycoplasma contamination. The cells were detached from the plates

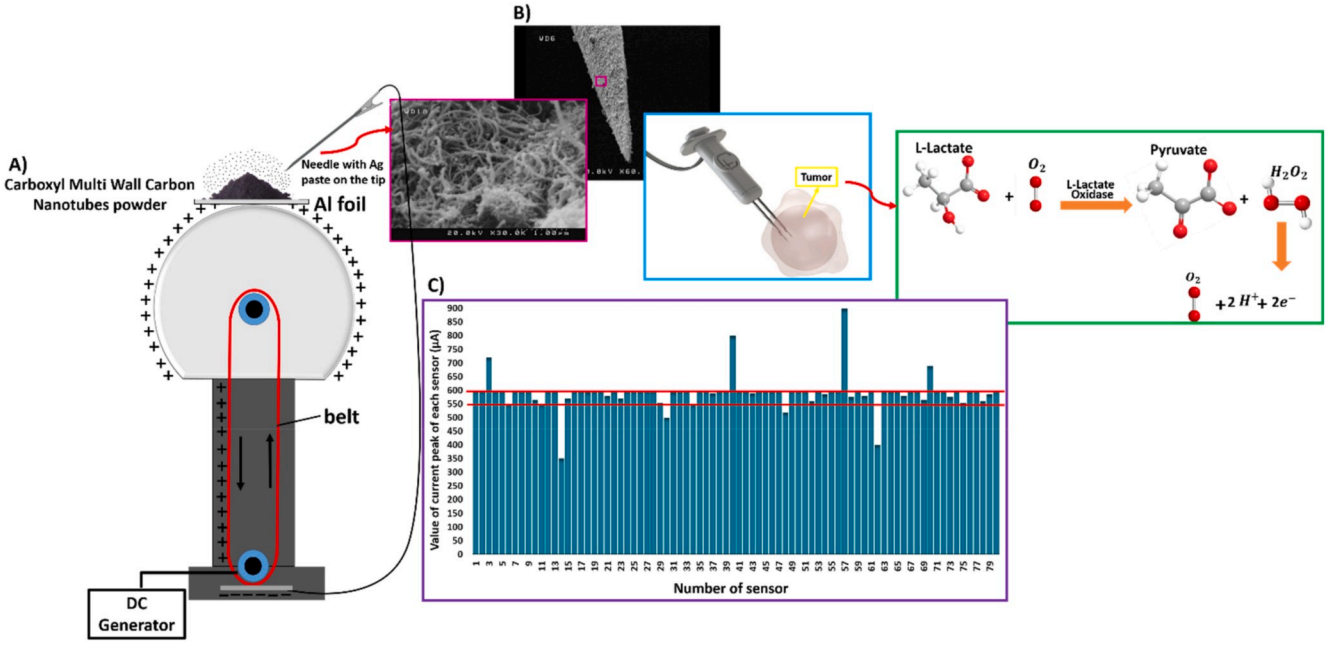

Fig. 1. A) Schematic of the deposition process of the CNT on the needle electrodes using a Van de Graaff, B) The needle electrode coated by multi wall carbon nanotubes presented in FESEM images. Distribution and abundance of nanotubes make a conformal surface for signal extraction, and C) Repeatability of the fabricated sensing needles was verified by testing more than 80 sensors on similar artificial tissues.

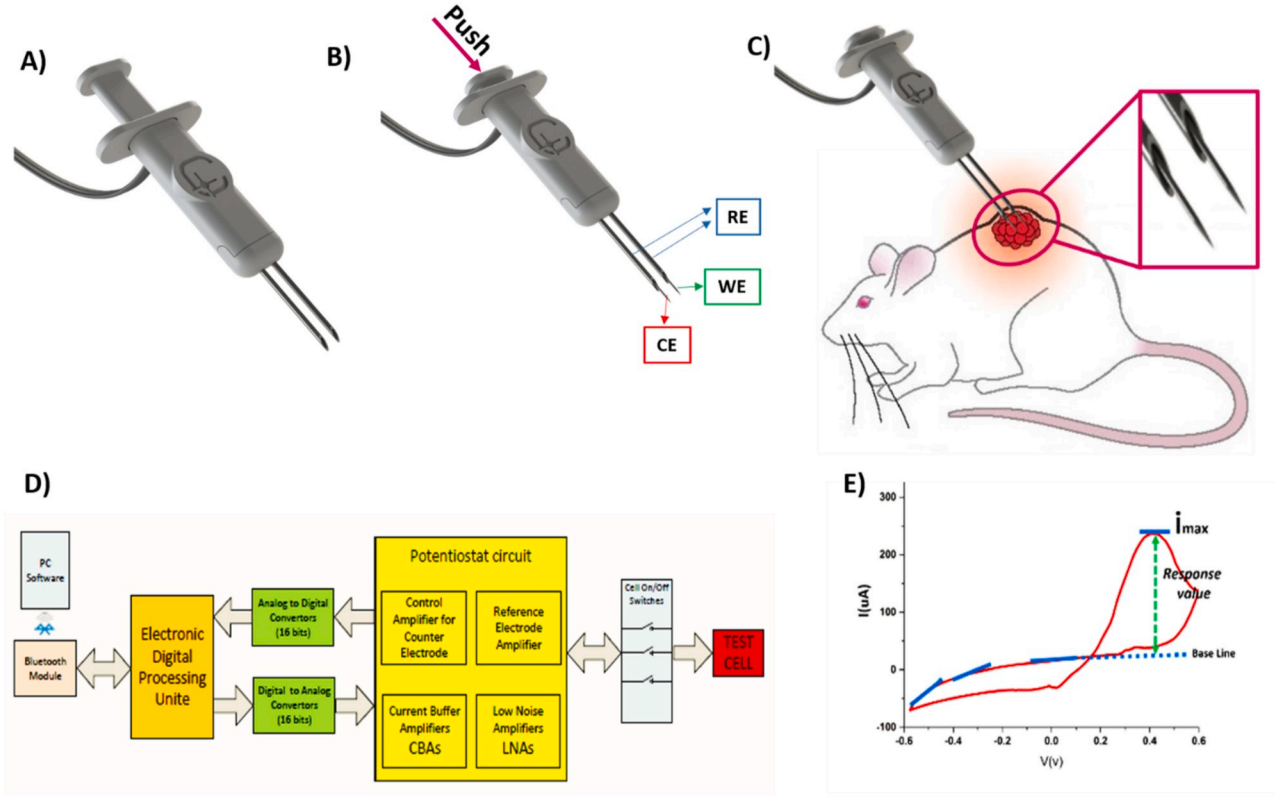

Fig. 2. The schematic of BGP, A) before and B) after pushing the WE and CE inner needles from the outer REs BGP, C) applying BGP to test the nature of a tumor had been candidate for biopsy, D) block diagram of integrated portable automatic electrochemical readout protocol of BGP board, and E) CV curve sample of the BGP response value.

by trypsin and counted by neobar laam.

2.4. Tumor formation in animal models

Female inbred BALB/c mice at 6–8 weeks of age were purchased from Pasteur Institute. They were kept at 22–24 °C with a 12 h light/

dark cycle in an utterly designed pathogen-free isolation facility and allowed to adapt for one week prior to experimentation. Our animal ethics committee approved all procedures. A total of 2×10^6 4T1 cells/200 μl in logarithmic growth phase were subcutaneously (s.c.) injected into the back neck or right side of BALB/c mice. Tumor size was measured using a portable sonogram. In the case of non-malignant tumor injection, a total of 2×10^6 MC4L2 cells/200 μl in logarithmic growth phase were subcutaneously (s.c.) injected into the right side of BALB/c mice.

2.5. Staining procedure od dissected tissues with hematoxylin eosin

Hematoxylin and Eosin (H&E) staining is the most common staining technique in histopathology. This method is a combination of two dyes. Hematoxylin and Eosin are used to demonstrate the nucleus and cytoplasmic inclusions in clinical specimens. Hematoxylin which contains Alum, acts as mordant and stains the nucleus light blue. In the presence of acid, the dye turns into red as a result, the differentiation is achieved by treating the tissue with acid solution. In the bluing step the initial soluble is converted to red color within the nucleus to an insoluble blue color. By utilizing eosin, the counterstaining is done which imparts pink color to the cytoplasm. The initial step of H&E staining process is deparaffinizing a tissue section and flaming the slide on burner and placing in the xylene. The process treatment must be repeated afterwards, the Hydration process must be done. In order to hydrate the tissue section, one should pass it through decreasing concentration of alcohol baths and water (100%, 90%, 80%, and 70%). Then the sample should be stained in hematoxylin for approximately 3–5 min followed by washing in running tap water until sections “blue” for 5 min or less. In the next step, for 5 min the sample should be differentiated in 1% acid alcohol (1% HCL in 70% alcohol). Subsequently, the sample should be washed in running tap water until it turns into blue again by dipping in an alkaline solution (e.g. ammonia water) followed by tap water wash. Furthermore, in 1% Eosin for 10 min the sample is stained and should be washed in tap water for 1–5 min. Finally, to dehydrate the sample, one should dip it in increasing concentration of alcohols and clear in xylene.

2.6. Statistical analysis

Data of this study were presented as means ± standard deviation (Mean ± S.D.). To assess the significance of the differences between the two experimental mice groups (G1 and G2), a statistical analysis was performed using Student’s t-test using Graph Pad Prism Software (V. 8.0.1) for repeated measurements with the significance assessed at the 5% significance level ($P < 0.05$).

3. Results and discussions

BGP consists of an integrated automatic electrochemical readout board. Sensing head probe was fabricated by adherence of electrostatically activated MWCNTs (with positive charges) on the tip of two steel needles (with the diameter of 250 μm) activated by negative electrostatic charges in the conformation of Working (WE) and Counter (CE) electrodes. The MWCNTs had been functionalized by carboxyl groups prior to attachment on electrodes. Two steel syringes with thickness of 0.5 mm used as reference electrodes (RE) which dynamically capped the WE and CE (Fig. 2B). REs was remained undecorated by CNTs. After entrance of REs (fabricated with the distance of 1–3 mm) into the suspicions mass, the WE and CE were pushed from the inside of REs into the tissues (Movie S1) to record the hypoxia related signals released from cancer cells. The sensors were sterilized under plasma sterilizer protocol (standard No: ISO/NP 22441). To evaluate the effect of plasma sterilization on the response of the fabricated sensors, 10 sensors were selected randomly and their CV responses of media solution were presented in Fig. S2B. As can be seen in the figure, it didn’t induce any perturbations on the function and response of the nanostructures.

It is well known that the release of hydrogen peroxide molecules is one of the sequential evidences during hypoxia assisted glycolysis of cancer cells (Lopez-Lázaro, 2007). The detection mechanism of BGP has been based on an electrochemical recording of the hypoxia related oxygen peroxide molecules released from suspicious tissues when they become broken on the CNT WE needle patented before (US patent pub no.: US20180299401). In this study, the type, abundance, distribution and adhering nature of CNTs on electrodes are modified. Such modifications made BGP more suitable in detecting the massive tumor in the depth of the breast suitable for tumor finding purposes.

3.1. Real-time in vivo testing of BGP

The principal objective of designing the BGP system was applying it for human breast biopsy to reduce the number of excisions in the traditional core needle biopsy method. The presence of a suspicious mass in the breast with Breast Imaging Reporting and Data System (BIRADs) of more than IVA (under sonography) is pre-requisite to conduct the biopsy (Lee et al., 2018). But before that, the system must be evaluated on animal models.

First, BGP was tested on different cellular secretions to evaluate their hypoxia-related electrochemical responses as an in vitro model. The comparative column chart of CV responses of media solution collected from two models of mice breast cancer cell lines (MC4L2 and 4T1), was presented in Supplementary Fig. 3. Before the test, the cells were cultured for 72 h in low oxygen ambient to better simulate the hypoxic ambient of the tumor environment. The test was carried out by injecting the electrodes to an artificial tissue (biological sponge) that had been immersed in the mentioned cellular media solution. The significant increase in the intensity of the cathodic peak from triple-positive primary grade (MC4L2) to triple-negative invasive grade (4T1) of the mice breast cancer cell lines was observed. These responses showed a direct correlation between the BGP current peak responses and invasive grades of the cancer cells in the in-vitro model. In the next step for determining the in-vivo tumor biosensing efficiency of BGP, 20 BALB/C female mice were divided into two cohort. One cohort was injected by $2*10^6$ 4T1 mouse-derived breast cancer cell lines for each mouse and the others were injected by the similar concentration of MC4L2 mouse derived breast cancer cell lines. 4T1 showed more invasive behavior without any response to hormone therapy in comparison with MC4L2 lines (Atiya et al., 2019), (Steenbrugge et al., 2016), (Steenbrugge et al., 2018). After tumor formation, the sonography was conducted to investigate the size and the probability of the presence of any necrosis in the tumors. We aimed to test non-necrotic tumors to better elaborate the electrochemical function of their hypoxic behavior. In the first step, the REs of BGP was entered to the tumor under the guidance of ultrasonography. After being ensured from the presence of the REs in the tumor, the WEs and CEs were pushed from inner of REs into the tumor and Cyclic Voltammetry (CV) signals were recorded. Then they were returned into the RE needles and the needles were exited from the body of mice (Movie S1). Similar tests were conducted on normal regions of the mice (Fig. 3). CV peaks presented in Fig. 4, showed the meaningful differences between CVs of normal and cancerous regions of both 4T1 and MC4L2 tumorized mice.

Experimental CV results were compared with histo-pathological patterns of the tested lesions and scaled ranges of the peak responses near the pathological scores of diagnostics were derived (Fig. 4). In this diagram, a gap of about 190 μA was observed between the BGP peaks of normal and cancer lesions (Fig. 4A). This means that lesions involved to 4T1 tumors showed BGP responses of more than 250 μA while normal tissues of such mice showed peak currents less than 60 μA. Such gap was about 50 μA in mice tumorized with MC4L2 cells which means that the cancer lesions showed BGP responses more than 105 μA and normal tissues less than 55 μA (Fig. 4B).

The BGP showed about 93% accuracy and 95% sensitivity in real-time in vivo detection of the breast tumors (Table S2).

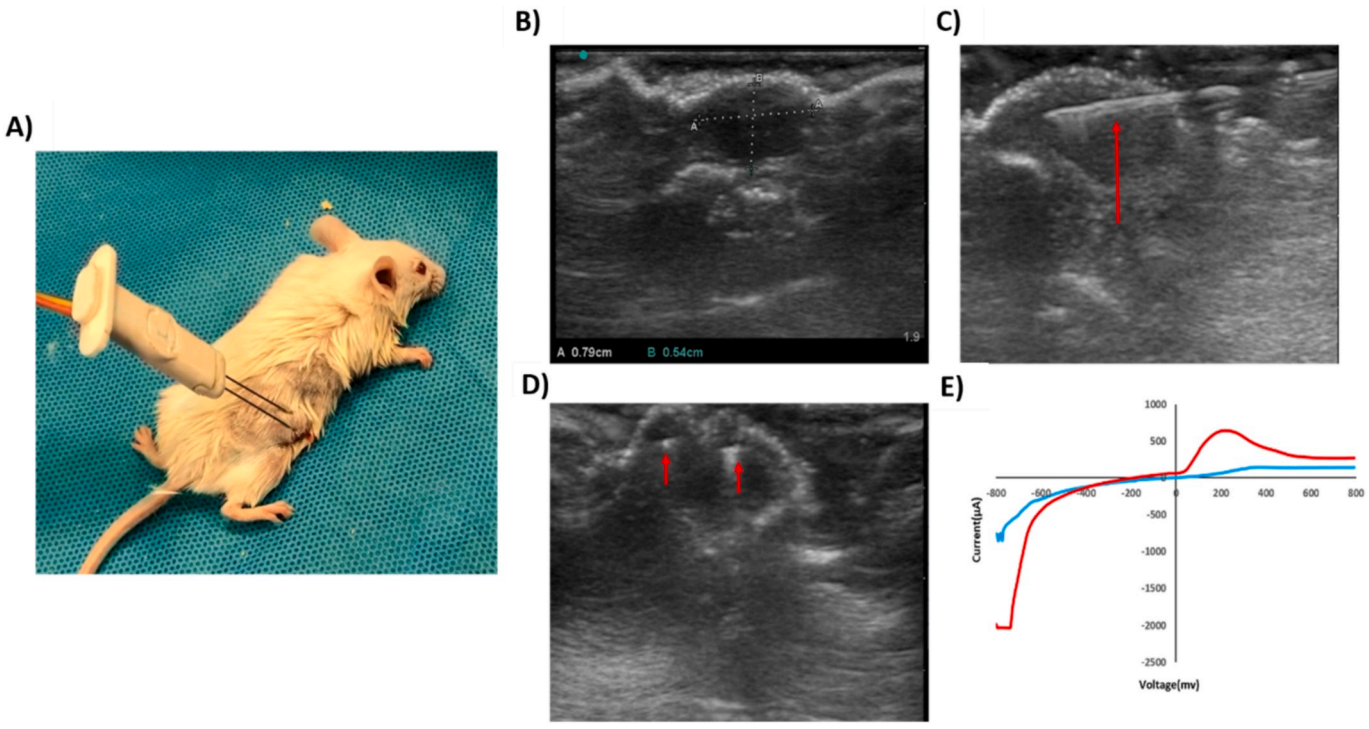

Fig. 3. A) Applying BGP to a mouse with the 4T1 breast cancer tumor, B) Tumor revealed by sonography image taken before testing by BGP, C) The sonography image of needles inside the tumor, D) Front view of BGF needles inside the tumor in sonography image and E) CV diagrams of normal and tumor regions, the CV current peaks were higher in cancer region vs. normal ones.

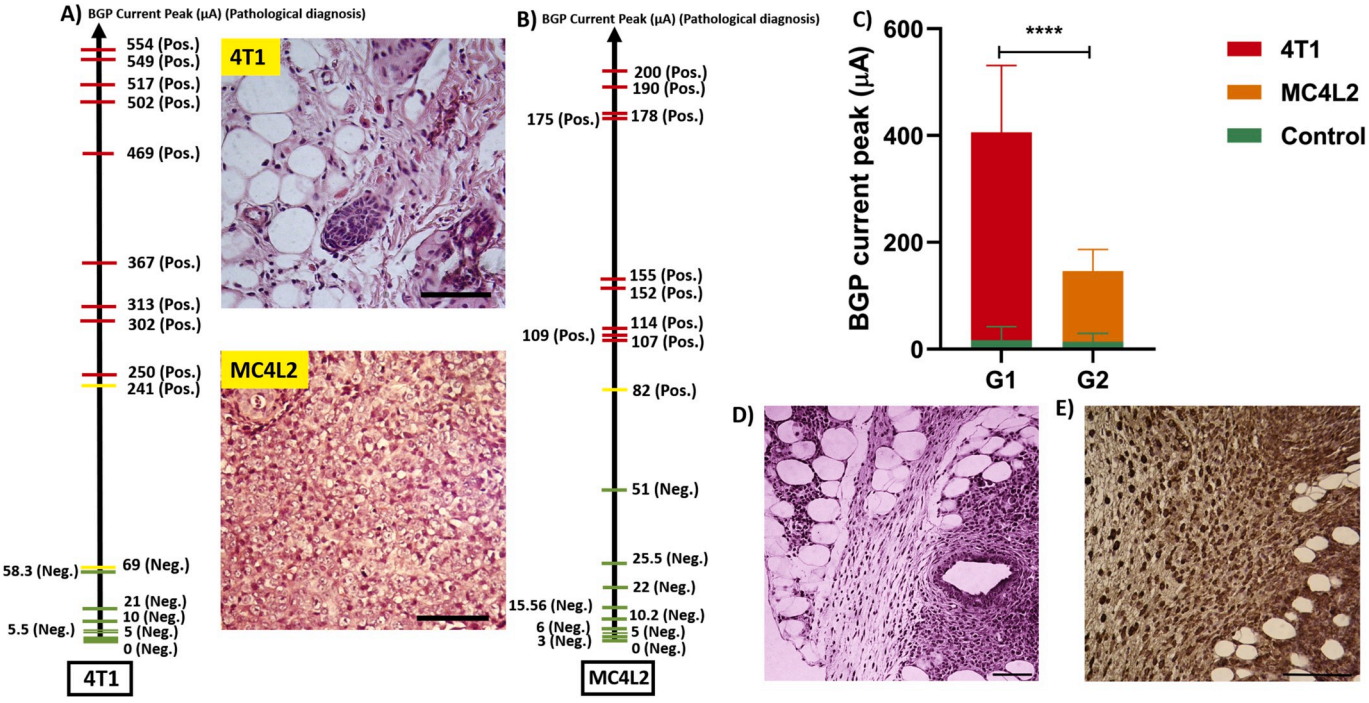

Fig. 4. CV peaks showed the meaning full differences between normal and cancerous regions of, A) 4T1 and B) MC4L2 tumors of mice. **Red color** refers to positive sample (Tumor), **Green color** is for negative sample (Normal regions) and **Yellow color** shows the samples that is not correctly evaluated by BGP (2 false positive and 1 false negative of BGP scores from 40 samples). Each scale bar in H&E image is equal to 100 μm, C) The comparative column chart of the BGP responses for 40 mice with MC4L2 and 4T1 tumors. The differences in BGP current peaks between 4T1, MC4L2 tumors and normal regions were highly significant (P value < 0.0001) (G1, G2 refers to tumor and normal regions of 4T1 and MC4L2 mice, respectively), D) H&E and E) HIF1 alpha IHC patterns of 4T1 tumors with BGP peak of 517 μA. (For interpretation of the references to color in this figure legend, the reader is referred to the Web version of this article.)

Moreover, the hypoxia associated peak levels of BGP in 4T1 tumors were higher than MC4L2 tumors. This result is in great correlation with higher hypoxic functions of 4T1 cell lines reported elsewhere (Hoffmann et al., 2018), (Serganova et al., 2018). Immunohistochemical (IHC) assay of 4T1 tumor showed that most of the cancer cells expressed the hypoxia-induced factor1-alpha (HIF1-α) (Gao et al., 2016) as an indication for their positive hypoxic functions (Fig. 4C and D).

Tumor tissues showed hypoxia glycolysis associated CV peaks in the ranges mentioned in Fig. 4 based on abundancy and vitality of cancer cells but normal tissues release much lower hypoxia associated H_2O_2 molecules. Hence, a neglectable peak would be observed. Depend on the location of normal (if it was in neighboring (margins) of the tumor or far from tumor lesion), some hypoxia associated diffused current might be recorded as false positive. Cancer-associated functions of neighbor normal tissues, such as field cancerization and cancer-associated fibroblast (Chai and Brown, 2009; Potter et al., 2016), might play role in CV peak responses of these neighbor tissues. So, normal fatty and skin tissues show very low peaks, muscle tissues show moderate peaks, tumor tissues show a very high peak, neighbor tissues to the tumor show peaks higher than normal tissues far from the tumor (Supplementary Fig. 4).

3.2. Finding necrotic regions of tumors by BGP

BGP also can be applied in detecting the vital state of the tumors. To evaluate this capability, the probe was tested on 4T1 tumors before and after it was treated by Electrochemical therapy (EChT) protocol (Sadighbayan et al., 2019). Treated 4T1 tumors showed very lower levels of CV peaks in comparison with its non-treated tumors (Fig. 5). H&E images confirmed the extensive necrosis in treated 4T1 tumors (dissected by biopsy) (Fig. 5C). It revealed that the therapeutic effects on the vitality of solid tumors could be monitored by BGP without any requirement for biopsy or expensive scans.

Those results show promising lights in applying BGP as an alternative or complementary tool to reduce the numbers and volumes of interventional sampling or expensive imaging.

3.3. Effect of functionalized CNTs as BGP sensing agents

The presence of functionalized CNTs with carboxyl groups drastically increase the quality and level of the peak current recorded by BGP. Similar tests done by non-CNT decorated steel electrodes and CNT electrodes without COOH functionalization (Fig. 6). Results revealed the impact of CNT in recording Hypoxia associated signals. CNT free electrodes (Steel needle electrodes) didn't show any distinctive response between normal and malignant lesions (Fig. 6A). Non-functionalized CNT electrodes showed acceptable response differences between normal and malignant lesions (Fig. 6B). Functionalized CNTs showed increased levels of current response in malignant lesions with respect to the non-functionalized electrode (better sensitivity). Also, it showed further differences in the current peaks between normal and malignant lesions (better specificity) (Fig. 6C). these are in corroboration with the facts that the carboxyl functionalization would increase the bonding sites with peroxide hydrogen molecules (Goran et al., 2015), (Zhou et al., 2019).

4. Conclusion

In summary, BGP was designed to find suspicious lesions to malignancy before doing core needle biopsy in solid tumors (even in the depth of the breast) based on the electrochemical recording of hypoxic functions. The peak level of BGP in tumor regions are much more than normal ones. Even it can distinct the vital tumor from necrotic tumors due to their different hypoxic functions. BGP can reduce the number of biopsied samples from non-malignant tissues diagnosed through their down-regulated hypoxia functions. Moreover, it can be applied for treatment monitoring instead of expensive imaging methods.

Although BGP would be proposed as a clinically usable sensor with pathological classification for the *in-vivo* diagnosis of benign and malignant tumors based on the hypoxia glycolysis functions of cancer cells, no experiments on human models with different types of cancer tumors might be its weaknesses that ought to be considered for future work.

Declaration of competing interest

The authors declare the following financial interests/personal relationships which may be considered as potential competing interests: Name of organization: Iran Nano Fund. Postal code: 1533984. Phone: +98 21 8876 9188. Email: info@nanofund.ir. Web page address: http://nanofund.ir.

Credit authorship contribution statement

Zohreh Sadat Miripour: Data curation, Formal analysis, Methodology, Investigation, Parisa Aghaee: Formal analysis, Methodology, Visualization, Fereshteh Abbasvandi: Methodology, Validation, Investigation, Parisa Hoseinpour: Methodology, Validation, Investigation, Hadi Ghafari: Methodology, Visualization, Naser Namdar: Formal analysis, Methodology, Validation, Mohammad Abdolahad:

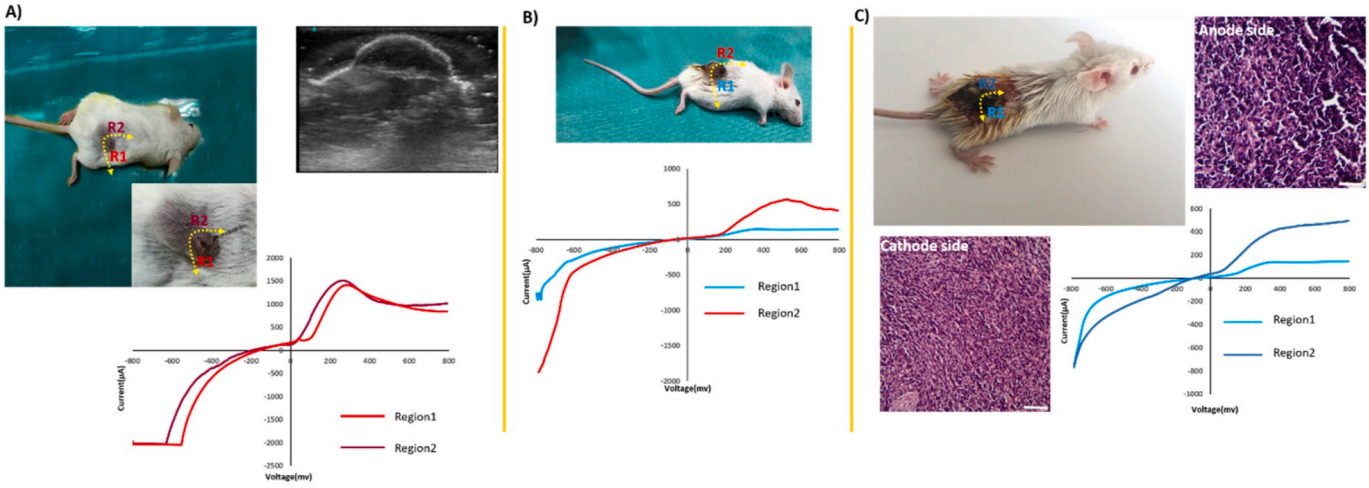

Fig. 5. BGP response and sonography image of 4T1 mice tumor, A) Before treatment by EChT, B) first treatment period (R1 region was treated) and C) second treatment cycle (R2 region was also treated), H&E images of EChT treated tumor showed extensive necrosis.

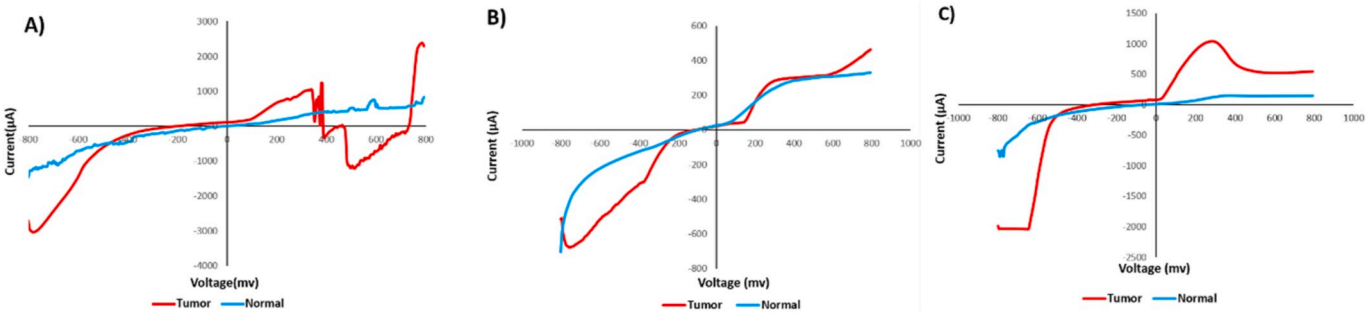

Fig. 6. BGP responses on normal and 4T1 tumor lesions of mice recorded by A) Non-CNT covered electrodes, B) Non-functionalized CNT electrodes and C) Functionalized CNT (carboxyl groups). BGP were entered to the normal and cancer tissues of mice for recording hypoxia associated signals.

Conceptualization, Formal analysis, Supervision, Project administration, Writing – original draft, Writing - review & editing. Mohammad esmaeil Akbari: design of probe for medical uses and biological test prerequisites.

Declaration of competing interest

The authors declare the following financial interests/personal relationships which may be considered as potential competing interests: Name of organization: Iran Nano Fund. Postal code: 1533984. Phone: +98 21 8876 9188. Email: info@nanofund.ir. Web page address: http://nanofund.ir.

Appendix A. Supplementary data

Supplementary data to this article can be found online at https://doi.org/10.1016/j.bios.2020.112209.

References

Ahn, S., Lee, J., Cho, M.-S., Park, S., Sung, S.H., 2017. Arch. Pathol. Lab Med. 142, 364–368.

American Cancer Society, 2019. Breast Cancer Facts & Figures 2019-2020. American Cancer Society, Inc, Atlanta. https://www.cancer.org/content/dam/cancer-org/research/cancer-facts-and-statistics/annual-cancer-facts-and-figures/2020/cancer-facts-and-figures-2020.pdf.

Atiya, H.I., Dvorkin-Gheva, A., Hassell, J., Patel, S., Parker, R.L., Hartstone-Rose, A., Hodge, J., Fan, D., Ramsdell, A.F., 2019. Anticancer Res. 39, 2277–2287.

Chai, H., Brown, R.E., 2009. Field effect in cancer-an update. Ann. Clin. Lab. Sci. 39, 331–337.

Dixon, J.M., Barber, M.D., 2018. Breast Surgery E-Book: A Companion to Specialist Surgical Practice. Elsevier Health Sciences.

Donaldson, A.R., McCarthy, C., Goraya, S., Pederson, H.J., Sturgis, C.D., Grobmyer, S.R., Calhoun, B.C., 2018. Cancer 124, 459–465.

Ehrenworth, A.M., Claiborne, T., Peralta-Yahya, P., 2017. Biochemistry 56, 5471–5475.

Gao, J.-L., Shui, Y.-M., Jiang, W., Huang, E.-Y., Shou, Q.-Y., Ji, X., He, B.-C., Lv, G.-Y., He, T.-C., 2016. Oncotarget 7, 71802.

Goran, J.M., Phan, E.N.H., Favela, C.A., Stevenson, K.J., 2015. Anal. Chem. 87, 5989–5996.

Halonen, S., Kari, J., Ahonen, P., Kronström, K., Hyttinen, J., 2019. Ann. Biomed. Eng. 47, 836–851.

Halter, R.J., Zhou, T., Meaney, P.M., Hartov, A., Barth Jr., R.J., Rosenkranz, K.M., Wells, W.A., Kogel, C.A., Borsic, A., Rizzo, E.J., 2009. Physiol. Meas. 30, S121.

Hoffmann, C., Mao, X., Brown-Clay, J., Moreau, F., Al Absi, A., Wurzer, H., Sousa, B., Schmitt, F., Berchem, G., Janji, B., 2018. Sci. Rep. 8, 10191.

Kılıç, F., Eren, A., Tunç, N., Velidedeoğlu, M., Bakan, S., Aydoğan, F., Çelik, V., Gazioğlu, E., Yılmaz, M.H., 2016. J. Breast Health 12, 25.

Lee, K.A., Talati, N., Oudsema, R., Steinberger, S., Margolies, L.R., 2018. Curr. Radiol. Rep. 6, 5.

Lopez-Lázaro, M., 2007. Canc. Lett. 252, 1–8.

Łukasiewicz, E., Ziemiecka, A., Jakubowski, W., Vojinovic, J., Bogucevska, M., Dobruch-Sobczak, K., 2017. J. Ultrason. 17, 267.

Mahr, R., Frunzke, J., 2016. Appl. Microbiol. Biotechnol. 100, 79–90.

Mishra, V., Bouayad, H., Schned, A., Hartov, A., Heaney, J., Halter, R.J., 2012. IEEE Trans. Biomed. Eng. 59, 3327–3336.

Ohashi, R., Matsubara, M., Watarai, Y., Yanagihara, K., Yamashita, K., Tsuchiya, S., Takei, H., Naito, Z., 2016. Breast Cancer 23, 675–683.

Peroza, E.A., Ewald, J.C., Parakkal, G., Skotheim, J.M., Zamboni, N., 2015. Anal. Biochem. 474, 1–7.

Michelle Potter, Emma Newport and Karl J. Morten N; Biochem Soc Trans (2016) 44 (5): 1499–1505.https://doi.org/10.1042/BST20160094.

Ravikumar, S., Baylon, M.G., Park, S.J., Choi, J., 2017. Microb. Cell Factories 16, 62.

Rogers, J.K., Taylor, N.D., Church, G.M., 2016. Curr. Opin. Biotechnol. 42, 84–91.

Sadighbayan, D., Sadighbayan, K., Tohid-Kia, M.R., Khosroushahi, A.Y., Hasanzadeh, M., 2019. TrAC Trends Anal. Chem. (Reference Ed.) 7, 26. https://doi.org/10.1016/j.trac.2019.07.020.

Serganova, I., Cohen, I.J., Vemuri, K., Shindo, M., Maeda, M., Mane, M., Moroz, E., Khanin, R., Satagopan, J., Koutcher, J.A., 2018. PLoS One 13, e0203965.

Shashaani, H., Faramarzpour, M., Hassanpour, M., Namdar, N., Alikhani, A., Abdolahad, M., 2016. Biosens. Bioelectron. 85, 363–370.

Singh, G.R., Rai, M.K., Singh, R., Kumar, B., Choudhary, V., Kumar, A., Singh, S.K., 2016. J. Evol. Med. Dent. Sci. 5, 4759–4763.

Spliethoff, J.W., Prevoo, W., Meier, M.A.J., de Jong, J., Klomp, H.M., Evers, D.J., Sterenborg, H.J.C.M., Lucassen, G.W., Hendriks, B.H.W., Ruers, T.J.M., 2016. Clin. Canc. Res. 22, 357–365.

Steenbrugge, J., Breyne, K., Denies, S., Dekimpe, M., Demeyere, K., De Wever, O., Vermeulen, P., Van Laere, S., Sanders, N.N., Meyer, E., 2016. J. Mammary Gland Biol. Neoplasia 21, 113–122.

Steenbrugge, J., Breyne, K., Demeyere, K., De Wever, O., Sanders, N.N., Van Den Broeck, W., Colpaert, C., Vermeulen, P., Van Laere, S., Meyer, E., 2018. J. Exp. Clin. Canc. Res. 37, 1–18.

Wang, L., 2018. Sensors 18, 655.

Wang, M., He, X., Chang, Y., Sun, G., Thabane, L., 2017. Breast 31, 157–166.

You, K., Park, S., Ryu, J.M., Kim, I., Lee, S.K., Yu, J., Kim, S.W., Nam, S.J., Lee, J.E., 2017. J. Breast Cancer 20, 297–303.

Zhang, J., Jensen, M.K., Keasling, J.D., 2015. Curr. Opin. Chem. Biol. 28, 1–8.

Zheng, B., Zuley, M.L., Sumkin, J.H., Catullo, V.J., Abrams, G.S., Rathfon, G.Y., Chough, D.M., Gruss, M.Z., Gur, D., 2008. Med. Phys. 35, 3041–3048.

Zhou, Y., Fang, Y., Ramasamy, R.P., 2019. Sensors 19, 392.